INTERNATIONAL JOURNAL OF ROBUST AND NONLINEAR CONTROL
Int. J. Robust Nonlinear Control 2015; **25**:3495–3514
Published online 5 December 2014 in Wiley Online Library (wileyonlinelibrary.com). DOI: 10.1002/rnc.3280

Fixed-structure robust controller design for chatter mitigation in high-speed milling

N. J. M. van Dijk[1,§], N. van de Wouw[2,*,†,‡] and H. Nijmeijer[2]

[1] *Philips Innovation Services, High Tech Campus 7, 5656 AE Eindhoven, The Netherlands*
[2] *Department of Mechanical Engineering, Eindhoven University of Technology, 5600 MB Eindhoven, The Netherlands*

SUMMARY

Chatter is an instability phenomenon in high-speed milling that limits machining productivity by the induction of tool vibrations, inferior machining accuracy, noise, and wear of machine components. In this paper, a fixed-structure active chatter control design methodology is proposed, which enables dedicated shaping of the chatter stability boundary such that working points of higher machining productivity become feasible while avoiding chatter. The control design problem is cast into a nonsmooth optimization problem, which is solved using bundle methods. Using this approach, fixed-structure dynamic (delayed) output feedback controllers can be synthesized. Distinct benefits of this approach are the a priori fixing of the controller order, the limitation of the control action, and the fact that no finite-dimensional model approximations and online chatter estimation techniques are required. All these benefits are important in milling practice. Representative examples illustrate the power of the proposed methodology in terms of increasing the chatter-free depth of cut, thereby enabling significant increases in machining productivity. Copyright © 2014 John Wiley & Sons, Ltd.

Received 6 December 2013; Revised 23 October 2014; Accepted 7 November 2014

KEY WORDS: robust control; delay systems; high-speed milling; machining chatter; fixed-order controller synthesis

1. INTRODUCTION

High-speed milling is a widely used manufacturing technique to produce, for example, moulds and dies or components for the aerospace industry. The productivity in milling is often limited by the occurrence of an instability phenomenon called (regenerative) chatter. Chatter results in heavy vibrations of the tool causing an inferior workpiece surface quality, rapid tool wear, and noise.

The occurrence of chatter can be visualized in so-called stability lobes diagrams SLD. In an SLD, the chatter stability boundary between a stable cut (i.e., without chatter) and an unstable cut (i.e., with chatter) is visualized in terms of two important machining parameters, namely, the spindle speed and depth of cut. Given the fact that chatter should be avoided at all times, the chatter boundary in the SLD represents a firm limit on the material removal rate (determined by the spindle speed and depth-of-cut). To overcome chatter vibrations in high-speed milling and, therewith, to enable the chatter-free increase of the material removal rate, dedicated active control strategies are required.

The chatter stability boundary can be altered by passively or actively adapting the machine dynamics. Passive chatter suppression techniques exist that use dampers [1] or vibration absorbers

*Correspondence to: N. van de Wouw, Eindhoven University of Technology, Department of Mechanical Engineering, 5600 MB Eindhoven, the Netherlands.
†E-mail: n.v.d.wouw@tue.nl
‡N. van de Wouw is also with the Department of Civil, Environmental & Geo- Engineering, University of Minnesota, Minneapolis, USA.
§N. J. M. van Dijk performed this work when affiliated with the Eindhoven University of Technology.

[2]. Passive dampers are relatively cheap and easy to implement and never destabilize the system. However, the practically achievable amount of damping is rather limited. Moreover, vibration absorbers require accurate tuning of their natural frequencies and, consequently, lack robustness to changing machining conditions. Active chatter control in milling has mainly been focused on active damping of the machine dynamics [3, 4] or workpiece [5]. Damping the machine or workpiece dynamics, either passively or actively, results in a uniform increase of the stability boundary for all spindle speeds.

To enable more dedicated shaping of the stability boundary (e.g., lifting the SLD locally around a specific spindle speed at which one desires to operate for the manufacturing of a certain product), the regenerative effect, which is inherent to the metal cutting process and which is the root cause for chatter, should be taken into account during chatter controller design. In [6, 7], active chatter control methodologies, taking the regenerative effect into account, have been developed in the case of turning. Recently, an active chatter control methodology for the high speed milling process is presented in [8], which has also been validated experimentally in [9].

Except for the work in [4, 8], all research on active chatter control is limited to low spindle speeds (i.e., below 5000 rpm). Moreover, all aforementioned research either does not include the regenerative effect during controller design or utilizes high-order finite-dimensional approximations of the milling model for controller design, yielding high-order controllers, which is disadvantageous from an implementation perspective. In this respect, it is important to note that relatively high frequencies play a role in the stabilization of chatter, which makes the implementation of high-order controllers prohibitive in practice.

This paper presents a controller design methodology, which can guarantee chatter-free milling operations in an a priori defined range of process parameters, such as spindle speed and depth of cut. The proposed model-based approach toward controller synthesis explicitly takes into account the regenerative effect responsible for chatter. As a consequence, the approach employs milling models in terms of a set of DDEs. We refrain from employing finite-dimensional approximations of the delay yielding high-order models and high-order controllers as proposed in [8]. Instead, we propose a design for low-order fixed-structure active chatter controllers for the milling process. The latter novel approach has two advantages: firstly, it avoids controller design and stability analysis based on only approximated models and, secondly, it avoids the use of high-order controllers, which is disadvantageous from an implementation perspective.

An important part of the controller design is the selection of the variable used for feedback, see [8]. In this reference, it has been advocated that so-called perturbation feedback (i.e., only feeding back the chatter vibrations as opposed to the full vibration of the milling machine) is favorable from the point of view of limiting the control action, which is important in practice. Hereto, online estimation techniques for the chatter vibrations are needed because these cannot be measured directly, see [8, 10]. In the current paper, we propose an alternative way to achieve such perturbation feedback while still only using measurements of the full vibrations of the milling machine. Hereto, we propose to employ delayed output feedback (sometimes referred to as Pyragas feedback [11]), which is beneficial from an implementation perspective.

In fixed-structure or fixed-order controller synthesis for time-delay systems, results are often obtained using a Lyapunov-based approach, see, for example, [12]. Lyapunov-based approaches allow the incorporation of a more general class of uncertainties, such as time-varying uncertainties. However, the resulting optimization problems are in the form of bilinear matrix inequalities where the number of unknown variables in general grows quadratically with the number of states [13], which may lead to computational issues. Moreover, generally, the application of a Lyapunov approach leads to conservative results. The usage of an eigenvalue-based approach can overcome these disadvantages as explained in [14]. Therefore, we employ such an eigenvalue-based approach in this paper.

The main contributions of this paper can be summarized as follows. Firstly, we propose a fixed-order controller design technique for the high-speed milling process. This technique guarantees the avoidance of chatter in a pre-defined range of working points (in terms of spindle speed and depth-of-cut). In this way, large increases in productivity (material removal rate) can be achieved while avoiding chatter. Secondly, the proposed control strategy has favorable properties from an

DOI: 10.1002/rnc

implementation perspective in three ways. Firstly, it allows the user to pre-specify the order of the controller and hence supports low-order controller design, which is desirable in a real-time implementation. Secondly, the proposed strategy limits the control action by employing so-called perturbation feedback, and, thirdly, it implements such perturbation feedback through delayed output-feedback, which avoids the need for online estimation of chatter vibrations. A preliminary version of this work has appeared in [15]. Additional contributions of the current paper with respect to [15] are the following: firstly, the synthesis methodology has been extended to accommodate the design of *delayed* output feedback control (which benefits explained in the preceding text); secondly, the inclusion of the design of *dynamic* output feedback chatter controllers (which can improve performance with respect to static controllers); thirdly, more details about the synthesis methodology and algorithm are provided; and, finally, other and more extensive application examples are presented.

The paper is organized as follows. Section 2 presents the model of the milling process. The problem setting is described in Section 3. The problem will be cast into a generalized plant formulation, which is discussed in Section 4. Section 5 presents the fixed-structure controller design methodology. Results for an illustrative example are presented in Section 6. Finally, conclusions are drawn in Section 7.

2. THE HIGH-SPEED MILLING PROCESS

This section presents a comprehensive model of the milling process and discusses (chatter-related) stability properties of the model. For more details regarding modelling and stability analysis of the milling process, including experimental validation, see, for example, [16–20].

2.1. *High-speed milling model*

In Figure 1, a schematic representation of the milling process is given. A block diagram of the milling process, with controller, is given in Figure 2. As can be seen from the block diagram, even without the controller, the milling process is a closed-loop position-driven process. The setpoint of the open-loop milling process is the predefined motion of the tool with respect to the workpiece, given in terms of the static chip thickness $h_{j,\text{stat}}(t) = f_z \sin\phi_j(t)$, where f_z is the feed per tooth and $\phi_j(t)$ the rotation angle of the j-th tooth of the tool with respect to the y (normal)

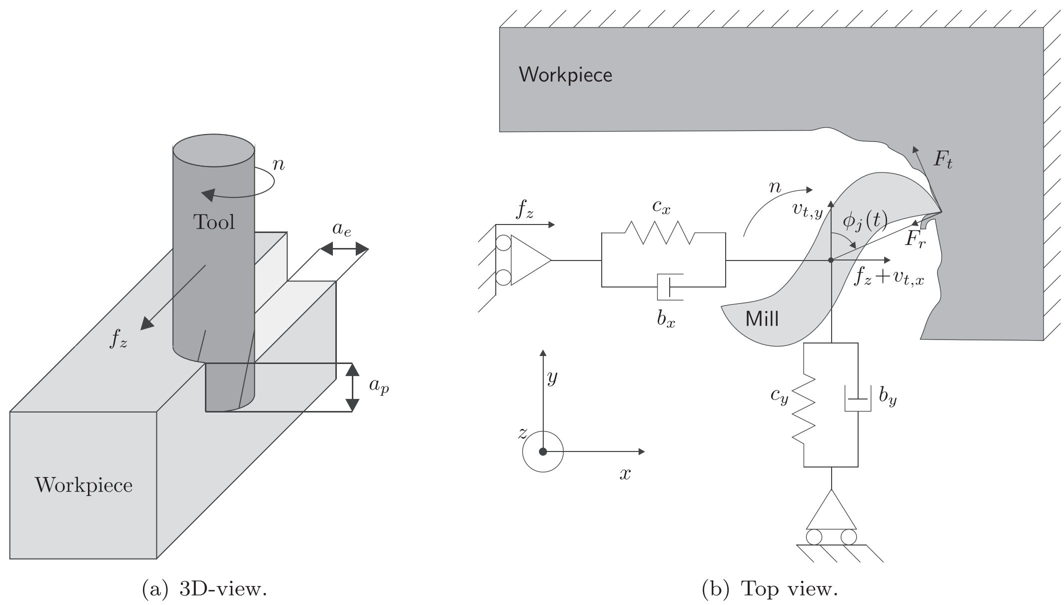

Figure 1. Schematic representation of the milling process.

DOI: 10.1002/rnc

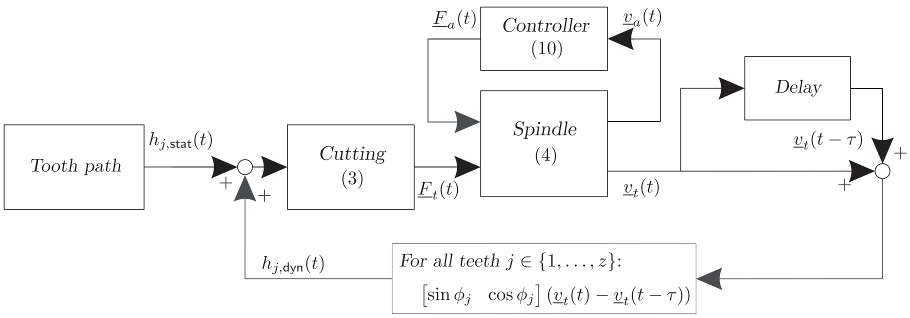

Figure 2. Block diagram of the milling process.

axis see (Figure 1(b)). However, the total chip thickness $h_j(t)$ also depends on the interaction between the cutter and the workpiece. This leads to cutter vibrations resulting in a dynamic displacement $\underline{v}_t(t) = \begin{bmatrix} v_{t,x}(t) & v_{t,y}(t) \end{bmatrix}^T$ of the tool, see Figure 1(b), which is superimposed on the predefined tool motion. This results in a wavy surface on the workpiece. The next tooth encounters the wavy surface, left behind by the previous tooth, and generates its own waviness. This is called the regenerative effect and results in the block *Delay* in Figure 2, see [21]. The difference between the current and previous wavy surface is denoted as the dynamic chip thickness $h_{j,\text{dyn}}(t) = \begin{bmatrix} \sin\phi_j(t) & \cos\phi_j(t) \end{bmatrix}(\underline{v}_t(t) - \underline{v}_t(t-\tau))$ with $\tau = 60/(zn)$ the delay, z the number of teeth, and n the spindle speed in revolutions per minute (rpm). Hence, the total chip thickness removed by tooth j at time $t, h_j(t)$, is the sum of the static and dynamic chip thickness: $h_j(t) = h_{j,\text{stat}}(t) + h_{j,\text{dyn}}(t)$.

The cutting force model (indicated by the *Cutting* block in Figure 2) relates the total chip thickness to the forces acting at the tool tip of the machine spindle. The forces in the tangential and radial directions, F_t and F_r in Figure 1(b), for a single tooth j are described by the following exponential cutting force model:

$$\begin{aligned} F_{t_j}(t) &= g_j(\phi_j(t))K_t\, a_p\, h_j(t)^{x_F}, \\ F_{r_j}(t) &= g_j(\phi_j(t))K_r\, a_p\, h_j(t)^{x_F}, \end{aligned} \tag{1}$$

where $0 < x_F \leqslant 1$ and $K_t, K_r > 0$ are cutting parameters, which depend on the workpiece material, and a_p is the axial depth of cut, see Figure 1(a). The function $g_j(\phi_j(t))$ in (1) describes whether a tooth is in or out of cut:

$$g_j(\phi_j(t)) = \begin{cases} 1, & \phi_s \leqslant \phi_j(t) \leqslant \phi_e \wedge h_j(t) > 0, \\ 0, & \text{else,} \end{cases} \tag{2}$$

where ϕ_s and ϕ_e are the entry and exit angle of the cut, respectively. Via trigonometric functions, the cutting force components in the x(feed) and y(normal) directions can be determined, see Figure 1(b). Hence, the total cutting forces in the x-direction and y-direction can be obtained by summing over all z teeth:

$$\underline{F}_t(t) = a_p \sum_{j=0}^{z-1} g_j(\phi_j(t)) \left(\left(h_{j,\text{stat}}(t) + \begin{bmatrix} \sin\phi_j(t) & \cos\phi_j(t) \end{bmatrix} (\underline{v}_t(t) - \underline{v}_t(t-\tau)) \right)^{x_F} \mathbf{S}(t) \begin{bmatrix} K_t \\ K_r \end{bmatrix} \right), \tag{3}$$

where

$$\mathbf{S}(t) = \begin{bmatrix} -\cos\phi_j(t) & -\sin\phi_j(t) \\ \sin\phi_j(t) & -\cos\phi_j(t) \end{bmatrix}.$$

The cutting force interacts with the spindle and tool dynamics (block *Spindle*) in Figure 2. The machine dynamics are modeled via a linear multi-input-multi-output (MIMO) state-space model,

DOI: 10.1002/rnc

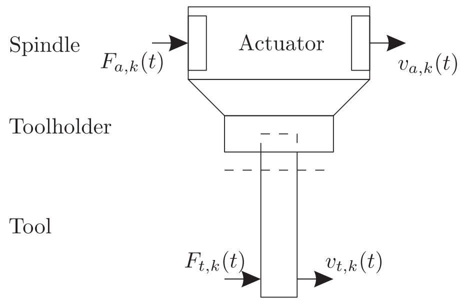

Figure 3. Schematic overview of spindle dynamics model, $k \in \{x, y\}$. $\underline{F}_a, \underline{v}_a$: forces, displacements at actuator. $\underline{F}_t, \underline{v}_t$: forces, displacements at tooltip.

$$\begin{aligned} \dot{\underline{x}}(t) &= \mathbf{A}\underline{x}(t) + \mathbf{B}_t \underline{F}_t(t) + \mathbf{B}_a \underline{F}_a(t), \\ \underline{v}_t(t) &= \mathbf{C}_t \underline{x}(t), \\ \underline{v}_a(t) &= \mathbf{C}_a \underline{x}(t), \end{aligned} \tag{4}$$

where $\underline{x}(t)$ is the state (the order of this model primarily depends on the order of the spindle-tool dynamics model) and cutting forces $\underline{F}_t(t) = \begin{bmatrix} F_{t,x}(t) & F_{t,y}(t) \end{bmatrix}^T$ given in (3), where $F_{t,x}(t)$ and $F_{t,y}(t)$ are the cutting forces in the x-direction and y-direction, respectively. The control forces are given by $\underline{F}_a(t) = \begin{bmatrix} F_{a,x}(t) & F_{a,y}(t) \end{bmatrix}^T$, where $F_{a,x}(t)$ and $F_{a,y}(t)$ are the control forces acting in the x-direction and y-direction, respectively, see Figure 3. In practice, the actuators used to induce these control forces are, for example, active magnetic bearings [4, 7, 9, 22]. Moreover, $\underline{v}_t(t)$ and $\underline{v}_a(t)$ represent the displacements of the cutter and the measured displacements available for feedback, respectively. The measured displacements $\underline{v}_a(t)$ are displacements in the spindle bearing, which can in practice, for example, be measured using eddy-current sensors [9].

Substitution of (3) into (4) yields the nonlinear, non-autonomous DDE describing the milling process:

$$\begin{aligned} \dot{\underline{x}}(t) &= \mathbf{A}\underline{x}(t) \\ &\quad + \mathbf{B}_t a_p \sum_{j=0}^{z-1} g_j(\phi_j(t)) \left(\left(h_{j,\text{stat}}(t) + \begin{bmatrix} \sin\phi_j(t) & \cos\phi_j(t) \end{bmatrix} \mathbf{C}_t (\underline{x}(t) - \underline{x}(t-\tau)) \right)^{x_F} \mathbf{S}(t) \begin{bmatrix} K_t \\ K_r \end{bmatrix} \right) \\ &\quad + \mathbf{B}_a \underline{F}_a(t), \\ \underline{v}_a(t) &= \mathbf{C}_a \underline{x}(t). \end{aligned} \tag{5}$$

2.2. *Stability of the milling process*

In this section, we briefly discuss the stability analysis of the milling process, where instability relates to the occurrence of the undesired chatter phenomenon.

In the milling process, the static chip thickness is periodic with time $\tau = \frac{60}{zn}$. Here, n is the spindle speed in rpm. In general, the uncontrolled (i.e., $\underline{F}_a(t) \equiv 0$) milling model (5) has a periodic solution $\underline{x}^*(t)$ with period time τ [23]. To validate this fact, let us adopt the following decomposition of $\underline{x}(t)$:

$$\underline{x}(t) = \underline{x}^*(t) + \tilde{\underline{x}}(t), \tag{6}$$

where $\underline{x}^*(t)$ is a τ-periodic motion that can be considered as the ideal motion when no chatter occurs and $\tilde{\underline{x}}(t)$ the perturbation term. When no chatter occurs, $\tilde{\underline{x}}(t) = 0$ and the tool motion is described by the following ODE:

$$\dot{\underline{x}}^*(t) = \mathbf{A}\underline{x}^*(t) + \mathbf{B}_t a_p \sum_{j=0}^{z-1} g_j(\phi_j(t)) h_{j,\text{stat}}(t)^{x_F} \mathbf{S}(t) \begin{bmatrix} K_t \\ K_r \end{bmatrix}, \tag{7}$$

DOI: 10.1002/rnc

which follows from (5) by exploiting the fact that $\underline{x}^*(t) = \underline{x}^*(t-\tau)\ \forall t$. The ODE in (7) represents a linear system with a periodic excitation with period time τ. Hence, when $\mathbf{A}$ has no eigenvalues at $\mathrm{i}l2\pi f_{tpe}$, for $f_{tpe} := \frac{1}{\tau}$ and all $l \in \mathbb{Z}$, the solution $\underline{x}^*(t)$ exists, is unique and is τ-periodic [24]. Chatter vibrations are related to oscillations in $\tilde{x}(t)$ and, hence, the periodic solution $x^*(t)$ is (at least locally) asymptotically stable when no chatter occurs and when chatter occurs it is unstable, see also [19]. Therefore, the chatter stability boundary can be found by studying the (local) asymptotic stability of the periodic solution $\underline{x}^*(t)$. To this end, the uncontrolled milling model is linearized about the periodic solution $\underline{x}^*(t)$, which yields the following linearised dynamics in terms of the perturbations $\underline{\tilde{x}}(t)$:

$$\begin{aligned}\dot{\underline{\tilde{x}}}(t) &= \mathbf{A}\underline{\tilde{x}}(t) + a_p\mathbf{B}_t\sum_{j=0}^{z-1}\mathbf{H}_j(t)\mathbf{C}_t\left(\underline{\tilde{x}}(t) - \underline{\tilde{x}}(t-\tau)\right) + \mathbf{B}_a\underline{F}_a(t),\\ \underline{\tilde{v}}_a(t) &= \mathbf{C}_a\underline{\tilde{x}}(t),\end{aligned} \tag{8}$$

where

$$\mathbf{H}_j(t) = g_j(\phi_j(t))x_F(f_z\sin\phi_j(t))^{x_F-1}\mathbf{S}(t)\begin{bmatrix}K_t\\K_r\end{bmatrix}\begin{bmatrix}\sin\phi_j(t) & \cos\phi_j(t)\end{bmatrix}. \tag{9}$$

As can be observed from (8) and (9), the linearised model is a delayed, periodically time-varying system. Stability of these kinds of systems can be assessed using, for example, the semi-discretization method of [25]. The main idea in semi-discretization is that only the delay term is discretized, instead of the actual time-domain terms. All stability lobes diagrams, presented throughout the paper, are determined using the semi-discretization method.

3. PROBLEM STATEMENT

As discussed in Section 1, the aim of this paper is to design a finite-dimensional fixed-structure linear controller $\mathbf{K}$ of low order to generate control inputs $\underline{F}_a$ based on measurements $\underline{v}_a$, which guarantees the following:

- robust stability of $\underline{\tilde{x}} = \underline{0}$ in (8), (9) for 'uncertainties' in depth of cut a_p and time delay τ;
- performance by minimizing the total amount of actuator energy needed to stabilize the milling process.

By guaranteeing robust stability for 'uncertainties' in a_p and τ, chatter-free milling operations can be guaranteed in an a priori defined range of spindle speeds n and depth of cut a_p. Moreover, limitation of the actuator forces will be included as a performance criterion in the controller design as it also is an important practical performance requirement. As discussed in [8], an important aspect in the active chatter control design procedure is the selection of the variable used for feedback. In [8], it is concluded that perturbation feedback (i.e., $\underline{\tilde{v}}_a$ is used as an input to the controller) is beneficial for reducing required actuator forces without compromising performance (in terms of the achievable closed-loop depth of cut/spindle speed interval for which chatter can be eliminated). In addition to such perturbation feedback, in this paper, we introduce dynamic *delayed* output feedback for robust stabilization of the high-speed milling process. As we will show in the succeeding text, by employing a specific form of dynamic *delayed* output feedback, no estimation algorithms are required to estimate the perturbation part $\underline{\tilde{v}}_a$ of the measured displacements $\underline{v}_a$ (as is the case with perturbation feedback, see [8]).

Then, the fixed-order controller $\mathbf{K}$, with input $\underline{\tilde{v}}_a \in \mathbb{R}^2$ and output (control action) $\underline{F}_a \in \mathbb{R}^2$, has the following state-space description:

$$\begin{aligned}\dot{\underline{\xi}}(t) &= \mathbf{A}_c\underline{\xi}(t) + \mathbf{B}_c\left(\underline{\tilde{v}}_a(t) - \beta\underline{\tilde{v}}_a(t-\tau)\right),\\ \underline{F}_a(t) &= \mathbf{C}_c\underline{\xi}(t) + \mathbf{D}_c\left(\underline{\tilde{v}}_a(t) - \beta\underline{\tilde{v}}_a(t-\tau)\right).\end{aligned} \tag{10}$$

Herein, $\underline{\xi} \in \mathbb{R}^{n_c}$, $\mathbf{A}_c \in \mathbb{R}^{n_c \times n_c}$, $\mathbf{B}_c \in \mathbb{R}^{n_c \times 2}$, $\mathbf{C}_c \in \mathbb{R}^{2 \times n_c}$, and $\mathbf{D_c} \in \mathbb{R}^{2\times 2}$ with n_c the order of the controller and $\beta \in \{0, 1\}$ a constant. For the sake of generality, we present both the case of delayed output feedback ($\beta = 1$) and the case of non-delayed output feedback ($\beta = 0$).

As mentioned before, the signal $\underline{\tilde{v}}_a(t)$ can typically not be measured directly. For the two cases of $\beta = 0$ and $\beta = 1$, the controller (10) can be implemented based on the measured spindle displacements $\underline{v}_a(t)$ as follows:

- If $\beta = 0$, we employ dynamic output feedback control and an online estimate of $\underline{\tilde{v}}_a(t)$ is needed, which can be obtained using measurements of $\underline{v}_a(t)$ and a chatter detection algorithm as presented in [10].
- If $\beta = 1$, we employ dynamic delayed output feedback. Then, by realising that $\underline{\tilde{v}}_a(t) - \underline{\tilde{v}}_a(t-\tau) = \underline{v}_a(t) - \underline{v}_a(t-\tau)$, because $v_a^*(t) = v_a^*(t-\tau)$ due to the periodic nature of the chatter-free solution, this controller can be directly implemented using only measurement of $\underline{v}_a(t)$ (without the need for online estimation algorithms to estimate the chatter vibrations $\underline{\tilde{v}}_a(t)$). The latter approach is pursued (so for $\beta = 1$) in this paper.

4. GENERALIZED PLANT FORMULATION

In order to solve the problem stated in the previous section, the model of the milling process will be extended with uncertainties in depth of cut a_p and spindle speed n. Hereto, the control goal will be cast into the generalized plant framework, see Figure 4. The generalized plant $\mathbf{P}$ is a given system with three sets of inputs and three sets of outputs. The signal pair $\underline{p}, \underline{q}$ denotes the inputs/outputs of the uncertainty channel connecting the plant to the uncertainty block $\mathbf{\Delta}$. The signal $\underline{r}$ represents an external input in which possible disturbances, measurement noise, and reference inputs are stacked. The signal $\underline{F}_a$ is the control input. The output $\underline{z}$ can be considered as a performance variable while $\underline{y}(t) = \mathbf{C}_a\left(\underline{\tilde{x}}(t) - \beta\underline{\tilde{x}}(t-\tau)\right)$ denotes the outputs used for feedback.

To derive the generalized plant formulation, first, a time-invariant approximation of the linearized model of the milling process (8) is employed. The focus in this work lies on full immersion cuts, where the full width of the cutter is used for cutting. As described in [16], for full immersion cuts, it is sufficient to average the dynamic cutting forces $\sum_{j=0}^{z-1}\mathbf{H}_j(t)$ over the tool path such that the milling model becomes an *autonomous* (time-invariant) DDE model. Because the cutter is only cutting when $\phi_s \leqslant \phi \leqslant \phi_e$, the averaged cutting forces are given by

$$\bar{\mathbf{H}} = \frac{z}{2\pi}\int_{\phi_s}^{\phi_e}\sum_{j=0}^{z-1}\mathbf{H}_j(\phi)\mathrm{d}\phi. \tag{11}$$

Then, the linear time-invariant model of the milling process is obtained by combining (8) with $\sum_{j=0}^{z-1}\mathbf{H}_j(t) = \bar{\mathbf{H}}$ and $\bar{\mathbf{H}}$ given in (11).

Based on the discussion aforementioned, let us define the following uncertainty sets:

$$a_p = \frac{1}{2}\bar{a}_p\left(1 + \delta_{a_p}\right), \tau = \tau_0 + \delta_\tau, \tag{12}$$

where $\bar{a}_p$ is the maximal depth of cut for which stable milling is desired, $\delta_{a_p} \in \mathbb{C},\ |\delta_{a_p}| \leqslant 1, \tau_0 = \frac{\bar{\tau}+\underline{\tau}}{2}$, and $\delta_\tau \in \frac{\bar{\tau}-\underline{\tau}}{2}[-1, 1]$, such that $0 < \underline{\tau} < \bar{\tau}$. Here, $\underline{\tau}$ and $\bar{\tau}$ together define the range of spindle

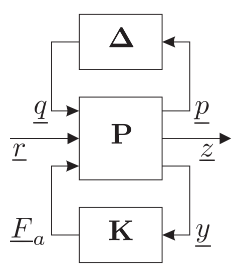

Figure 4. Generalized plant interconnection.

DOI: 10.1002/rnc

speeds $\left[\frac{60}{z\bar{\tau}}, \frac{60}{z\underline{\tau}}\right]$ for which stable milling is desired. Moreover, as described in Section 3, it is desired to limit the magnitude of the actuator forces. Therefore, the performance output is chosen as the weighted control input $\underline{z}(s) = \mathbf{W}_{KS}(s)\underline{F}_a(s)$, $s \in \mathbb{C}$, where $\mathbf{W}_{KS}$ is a stable weighting filter with the following state-space realization:

$$\begin{aligned} \dot{\underline{x}}_{KS}(t) &= \mathbf{A}_{KS}\underline{x}_{KS}(t) + \mathbf{B}_{KS}\underline{F}_a(t), \\ \underline{z}(t) &= \mathbf{C}_{KS}\underline{x}_{KS}(t) + \mathbf{D}_{KS}\underline{F}_a(t). \end{aligned} \tag{13}$$

Substituting (12) in (8) with $\sum_{j=0}^{z-1}\mathbf{H}_j(t)) = \bar{\mathbf{H}}$ and $\bar{\mathbf{H}}$ given in (11) and by adding the performance input/output channels to the system and rearranging terms, the state-space representation of the generalized plant $\mathbf{P}$ is given as follows[‡]:

$$\begin{aligned} \dot{\underline{x}}_P(t) &= \mathbf{A}_{P,0}\underline{x}_P(t) + \mathbf{A}_{P,1}\underline{x}_P(t-\tau_0) + \mathbf{B}_P\underline{u}_P(t) \\ \underline{v}_P(t) &= \mathbf{C}_{P,0}\underline{x}_P(t) + \mathbf{C}_{P,1}\underline{x}_P(t-\tau_0) + \mathbf{D}_P\underline{u}_P(t) \end{aligned} \tag{14}$$

with the state vector $\underline{x}_P(t) = \left[\tilde{\underline{x}}^T(t)\ \underline{x}_{KS}^T(t)\right]^T$, input vector $\underline{u}_P(t) = \left[\underline{q}^T(t)\ \underline{r}^T(t)\ \underline{F}_a^T(t)\right]^T$, with $\underline{r} \in \mathbb{R}^2$ representing measurement noise on the output $\underline{y}$, and output vector $\underline{v}_P(t) = \left[\underline{p}^T(t)\ \underline{z}^T(t)\ \underline{y}^T(t)\right]^T$. The (structured) uncertainty channel input $\underline{p}(t)$ and output $\underline{q}(t)$ are defined as

$$\underline{p}(t) = \begin{bmatrix} \underline{p}_1(t) \\ \underline{p}_2(t) \\ \underline{p}_3(t) \end{bmatrix} := \begin{bmatrix} \mathbf{C}_t\underline{x}(t-\tau_0) \\ \mathbf{C}_a\underline{x}(t-\tau_0) \\ \frac{1}{2}\bar{a}_p\mathbf{C}_t\left(\underline{x}(t) - \underline{x}(t-\tau_0)\right) - \frac{1}{2}\bar{a}_p q_1(t) \end{bmatrix}, \tag{15}$$

$$\underline{q}(t) = \begin{bmatrix} \underline{q}_1(t) \\ \underline{q}_2(t) \\ \underline{q}_3(t) \end{bmatrix} := \begin{bmatrix} \left(\mathcal{D}_{\delta_\tau} - 1\right)\underline{p}_1(t) \\ \left(\mathcal{D}_{\delta_\tau} - 1\right)\underline{p}_2(t) \\ \delta a_p \underline{p}_3(t) \end{bmatrix}, \tag{16}$$

where the delay-operator $\mathcal{D}_{\delta_\tau}$ is defined as $\mathcal{D}_{\delta_\tau}\underline{x}(t) = \underline{x}(t-\delta_\tau)$. The state-space matrices of the generalized plant in (14) are given by

$$\begin{aligned}
\mathbf{A}_{P,0} &= \begin{bmatrix} \mathbf{A} + \frac{1}{2}\bar{a}_p\mathbf{B}_t\bar{\mathbf{H}}\mathbf{C}_t & \mathbf{0} \\ \mathbf{0} & \mathbf{A}_{KS} \end{bmatrix},\ \mathbf{A}_{P,1} = \begin{bmatrix} -\frac{1}{2}\bar{a}_p\mathbf{B}_t\bar{\mathbf{H}}\mathbf{C}_t & \mathbf{0} \\ \mathbf{0} & \mathbf{0} \end{bmatrix}, \\
\mathbf{B}_P &= \left[\begin{array}{ccc|cc} -\frac{1}{2}\bar{a}_p\mathbf{B}_t\bar{\mathbf{H}} & \mathbf{0} & \mathbf{B}_t\bar{\mathbf{H}} & \mathbf{0} & \mathbf{B}_a \\ \mathbf{0} & \mathbf{0} & \mathbf{0} & \mathbf{0} & \mathbf{B}_{KS} \end{array}\right], \\
\mathbf{C}_{P,0} &= \left[\begin{array}{cc} \mathbf{0} & \mathbf{0} \\ \mathbf{0} & \mathbf{0} \\ \frac{1}{2}\bar{a}_p\mathbf{C}_t & \mathbf{0} \\ \hline \mathbf{0} & \mathbf{C}_{KS} \\ \mathbf{C}_a & \mathbf{0} \end{array}\right],\ \mathbf{C}_{P,1} = \left[\begin{array}{cc} \mathbf{C}_t & \mathbf{0} \\ \mathbf{C}_a & \mathbf{0} \\ -\frac{1}{2}\bar{a}_p\mathbf{C}_t & \mathbf{0} \\ \hline \mathbf{0} & \mathbf{0} \\ -\beta\mathbf{C}_a & \mathbf{0} \end{array}\right], \\
\mathbf{D}_P &= \left[\begin{array}{ccc|cc} \mathbf{0} & \mathbf{0} & \mathbf{0} & \mathbf{0} & \mathbf{0} \\ \mathbf{0} & \mathbf{0} & \mathbf{0} & \mathbf{0} & \mathbf{0} \\ -\frac{1}{2}\bar{a}_p\mathbf{I}_2 & \mathbf{0} & \mathbf{0} & \mathbf{0} & \mathbf{0} \\ \hline \mathbf{0} & \mathbf{0} & \mathbf{0} & \mathbf{0} & \mathbf{D}_{KS} \\ \mathbf{0} & -\beta\mathbf{I}_2 & \mathbf{0} & \mathbf{I}_2 & \mathbf{0} \end{array}\right]
\end{aligned}$$

with identity matrix $\mathbf{I}_n \in \mathbb{R}^{n\times n}$.

[‡]We employ ideas from [26] in constructing the generalized plant formulation.

DOI: 10.1002/rnc

In the following discussion, the transfer function description of the generalized plant will also be used. The transfer function description of the generalized plant $\mathbf{P}$ is given as follows:

$$\mathbf{P}(s) = (\mathbf{C}_{P,0} + \mathbf{C}_{P,1}e^{-s\tau_0})\,[s\mathbf{I} - \mathbf{A}_{P,0} - \mathbf{A}_{P,1}e^{-s\tau_0}]^{-1}\,\mathbf{B}_P + \mathbf{D}_P, \tag{17}$$

$s \in \mathbb{C}$.

Let $\mathbf{\Delta}(s)$ denote the Laplace transform of the uncertainty term (16), such that $\underline{q}(s) = \mathbf{\Delta}(s)\underline{p}(s)$ with

$$\mathbf{\Delta}(s) = \begin{bmatrix} \left(e^{-s\delta_\tau} - 1\right)\mathbf{I}_4 & \mathbf{0} \\ \mathbf{0} & \delta_{a_p}\mathbf{I}_2 \end{bmatrix}. \tag{18}$$

It can be seen that the uncertainty term, given in the preceding text, depends on the frequency. In [27], it has been shown that the delay uncertainty $e^{-s\delta_\tau} - 1$ can be upper bounded by a (non-rational) frequency-dependent upper bound $\kappa(i\omega)$ given as follows:

$$\kappa(\omega) = \begin{cases} 2\sin\frac{\delta_\tau\omega}{2}, & \forall\omega,\ 0 \leqslant \omega \leqslant \pi/\delta_\tau \\ 2, & \forall\omega \geqslant \pi/\delta_\tau, \end{cases} \tag{19}$$

in the sense that $\left|e^{-i\omega\delta_\tau} - 1\right| \leqslant \kappa(\omega)$. Let us define $\mathbf{L}(s) = \mathrm{diag}(\kappa(\omega)\mathbf{I}_4, \mathbf{I}_2)$, for all $s = \xi + i\omega, \xi, \omega \in \mathbb{R}$. Then the (scaled) generalized plant and uncertainty term is obtained as follows:

$$\tilde{\mathbf{P}}(s) = \mathrm{diag}(\mathbf{L}(s), \mathbf{I}_2, \mathbf{I}_2)\mathbf{P}(s),\ \ \tilde{\mathbf{\Delta}} = \mathbf{\Delta}(s)\mathbf{L}^{-1}(s).$$

5. SYNTHESIS OF FIXED-STRUCTURE DELAYED OUTPUT FEEDBACK CONTROLLERS

In this section, we propose a synthesis technique for the design of fixed-structure (delayed) output feedback controllers guaranteeing robust stability and performance. Based on the discussion in the previous section, it becomes clear that the design of a controller guaranteeing such robustness properties requires the following optimization problem to be solved:

$$\begin{gathered} \min_{\mathbf{K}} \sup_{\omega\in\mathbb{R}} \mu_{\tilde{\mathbf{\Delta}}}(\mathbf{N}), \\ \text{subject to } \Psi(\mathbf{K}) < 0, \end{gathered} \tag{20}$$

with $\mathbf{N}$ the lower fractional transformation LFT of $\tilde{\mathbf{P}}$ and fixed-structure controller $\mathbf{K}$ (see [28] for the definition of LFTs) and $\Psi(\mathbf{K})$ the spectral abscissa function of the closed-loop system defined as

$$\Psi(\mathbf{K}) := \sup\left\{\Re(\lambda) : \det\left(\lambda\mathbf{I} - \bar{\mathbf{A}}_0 - \bar{\mathbf{A}}_1 e^{-\lambda\tau_0}\right) = 0\right\}, \tag{21}$$

where

$$\bar{\mathbf{A}}_0 = \begin{bmatrix} \mathbf{A} + \frac{1}{2}\bar{a}_p\mathbf{B}_t\bar{\mathbf{H}}\mathbf{C}_t & \mathbf{0} \\ \mathbf{0} & \mathbf{0} \end{bmatrix} + \begin{bmatrix} \mathbf{B}_a & \mathbf{0} \\ \mathbf{0} & \mathbf{I} \end{bmatrix}\begin{bmatrix} \mathbf{D}_c & \mathbf{C}_c \\ \mathbf{B}_c & \mathbf{A}_c \end{bmatrix}\begin{bmatrix} \mathbf{C}_a & \mathbf{0} \\ \mathbf{0} & \mathbf{I} \end{bmatrix},$$

$$\bar{\mathbf{A}}_1 = \begin{bmatrix} -\frac{1}{2}\bar{a}_p\mathbf{B}_t\bar{\mathbf{H}}\mathbf{C}_t & \mathbf{0} \\ \mathbf{0} & \mathbf{0} \end{bmatrix} + \begin{bmatrix} \mathbf{B}_a & \mathbf{0} \\ \mathbf{0} & \mathbf{I} \end{bmatrix}\begin{bmatrix} \mathbf{D}_c & \mathbf{C}_c \\ \mathbf{B}_c & \mathbf{A}_c \end{bmatrix}\begin{bmatrix} -\beta\mathbf{C}_a & \mathbf{0} \\ \mathbf{0} & \mathbf{0} \end{bmatrix}.$$

The constraint on the objective function, defined in the preceding text, is a necessary condition to guarantee the existence of the $\mathcal{H}_\infty$-norm of $\mathbf{N}$ along with stability of the closed-loop system, see also [28].

The robust stability and performance requirement can now be translated into demanding that the objective function in (20) is smaller than one. It is in general difficult to calculate $\mu_{\tilde{\mathbf{\Delta}}}(\mathbf{N})$. However, an upper bound on $\mu_{\tilde{\mathbf{\Delta}}}(\mathbf{N})$ can be obtained by calculating the scaled $\mathcal{H}_\infty$ norm of $\mathbf{N}$ [28]. Because the uncertainties are modelled by complex uncertainties, see (12) and (18), as described in

DOI: 10.1002/rnc

the previous section, a reasonable approach to solve the problem is to apply D-K-iteration, see [28]. Hereby, the optimization problem is given as follows:

$$\begin{aligned} &\min_{\mathbf{K}} \inf_{\mathbf{D}\in\mathcal{H}_\infty} \left\| \mathbf{D}\mathbf{N}\mathbf{D}^{-1} \right\|_\infty, \\ &\text{subject to } \Psi(\mathbf{K}) < 0, \end{aligned} \tag{22}$$

which is iteratively solved for $\mathbf{K}$ and $\mathbf{D}$. Herein,

$$\left\| \mathbf{D}\mathbf{N}\mathbf{D}^{-1} \right\|_\infty = \sup_{\omega\in\mathbb{R}} \bar{\sigma}\left(\mathbf{D}(i\omega)\mathbf{N}(i\omega)\mathbf{D}(i\omega)^{-1}\right),$$

$\mathcal{H}_\infty$ denotes the set of functions that are analytic and bounded in the open right half plane, and the structure of $\mathbf{D}$ is chosen such that $\mathbf{D}$ commutes with the uncertainty set $\tilde{\mathbf{\Delta}}$, that is, satisfies $\mathbf{D}\tilde{\mathbf{\Delta}} = \tilde{\mathbf{\Delta}}\mathbf{D}$. We refer to, for example, [29] for more details on the computation of lower and upper bounds on the complex structured singular value. For a given $\mathbf{K}$, the problem of finding the scaling matrix $\mathbf{D}$ can be turned into a convex optimization problem, which is generally solved pointwise in the frequency domain (for example, by using the `mussv` command from the Robust Control Toolbox of MATLAB [30], which uses the algorithm presented in [31]). Because our aim is to design fixed-structure controllers, the problem of finding $\mathbf{K}$, for a given $\mathbf{D}$, in general results in a non-convex, non-smooth, constrained optimization problem, given as follows:

$$\min_{\mathbf{K}} f(\mathbf{K}), \text{ subject to } \Psi(\mathbf{K}) < 0 \tag{23}$$

with $f(\mathbf{K}) := \sup_{\omega\in\mathbb{R}} \bar{\sigma}\left(\mathbf{D}(i\omega)\mathbf{N}(i\omega)\mathbf{D}(i\omega)^{-1}\right)$.

The non-smooth dependence of the objective function (23) on the controller parameters of $\mathbf{K}$ typically occurs when the maximum of the objective function is located at two (or more) different frequencies. Due to the non-smoothness in (23), standard optimization algorithms cannot be used to determine the (optimal) parameters of controller $\mathbf{K}$, because these tend to chatter about a non-smooth surface. Instead, non-smooth optimization techniques, based on bundle methods [32, 33], will be used. Here, we employ a particular gradient bundle method, called gradient sampling, developed by Burke *et al*. [34]. In this way, when the optimization approaches a non-smooth manifold, at which, for example, a (smooth) steepest descent based algorithm will fail, the bundle algorithm is able to use the information from both sides of the non-smooth manifold to *turn the corner* and make progress toward the minimizer [35].

The gradient sampling algorithm can be used to locally minimize non-smooth, non-convex objective functions. In general, the gradient sampling algorithm is, however, quite expensive per iteration. Therefore, Lewis and Overlon have developed a hybrid algorithm for non-smooth optimization HANSO [36]. First, the BFGS method (named after its inventors Broyden, Fletcher, Goldfarb, and Shannon), a quasi-Newton algorithm, with an inexact line search algorithm based on weak Wolfe conditions is employed (see [37] for detail on BFGS and line search methods). When the BFGS algorithm finds a minimizer, the optimization is stopped. In the event that, at a certain iteration, the Wolfe conditions are not satisfied, which indicates that the optimization is near a non-smooth manifold, the gradient sampling algorithm is employed where the sampling radius is adaptively reduced, see [34].

The hybrid optimization algorithm HANSO, as discussed in the preceding text, is in general applied to finite-dimensional systems with continuous objective functions. However, as shown in [14, Chp. 9], the $\mathcal{H}_\infty$-norm of a system with time delay exhibits continuity properties and is differentiable almost everywhere, which allows the application of HANSO for the present problem.

From (23), it can be seen that the problem of finding a fixed-structure controller, which guarantees robust performance of the milling process is actually a *constrained* optimization problem. However, HANSO is only able to deal with unconstrained optimization problems. The constrained optimization problem can, however, be converted to an unconstrained optimization problem using a penalty method, see [38]. Hence, in this paper, we opt to replace the constrained objective function

DOI: 10.1002/rnc

in (23) with an unconstrained (non-smooth) objective function, yielding the following unconstrained optimization problem:

$$\min_{\mathbf{K}} \bar{f}(\mathbf{K}), \tag{24}$$

where $\bar{f}(\mathbf{K}) = f(\mathbf{K}) + \gamma \max(0, \Psi(\mathbf{K}))$ and γ is a positive constant. The value of γ is in general iteratively chosen, see [37] for rules on how to choose γ.

During an optimization step, in order to evaluate the objective function (24) for given $\mathbf{K}$ and $\mathbf{D}$, the (scaled) $\mathcal{H}_\infty$-norm of $\mathbf{DND}^{-1}$ as well as spectral abscissa $\Psi(\mathbf{K})$, defined in (21), needs to be calculated. Because, in this case, the system is infinite dimensional (due to the presence of the time delay), the standard Hamiltonian approach to calculate the $\mathcal{H}_\infty$-norm, as presented in [39], cannot be used. Recently, in [40], a method is presented to compute the $\mathcal{H}_\infty$-norm of a stable time-delay system with transfer function representation

$$\mathbf{G}(s) = \mathbf{C}\left(s\mathbf{I} - \mathbf{A}_0 - \mathbf{A}_1 e^{-s\tau}\right)^{-1} \mathbf{B} + \mathbf{D}. \tag{25}$$

Unfortunately, as can be seen from (17), the transfer function description of the generalized plant is not in the form of (25). Hence, here, the $\mathcal{H}_\infty$-norm will be determined by calculating the singular values of $\mathbf{D}(i\omega)\mathbf{N}(i\omega), \mathbf{K}(i\omega))\mathbf{D}(i\omega)^{-1}$ pointwise across a grid of frequencies $\underline{\omega} = [\omega_1, \omega_2, \ldots, \omega_N]^T$. The spectral abscissa is determined using the DDE-BIFTOOL [41] software package, which can be used to determine the right-most characteristic roots of an LTI system with time delays. More information about computation of characteristic roots for time-delay systems can be found in [14].

Based on the discussion in the preceding text, an algorithm is devised to solve the fixed-structure robust control synthesis problem for LTI time-delay systems with structured uncertainties, see [9] for further details on this algorithm and the role of gradient sampling herein. Finally, we remark that, because the controller synthesis problem posed in the preceding text is in general a non-convex problem, the choice of the initial controller parameters, used as input for the fixed-order controller synthesis procedure, requires careful consideration. As argued in [7, 8, 42], and confirmed by the results in Section 6, it is beneficial to design a controller that changes the closed-loop spindle dynamics in such a way that the dominant natural frequency of the (closed-loop) spindle dynamics is close to a tooth passing excitation frequency. Therefore, it is desirable to choose initial controller parameters inducing such desirable closed-loop characteristics at least approximately. This could, for example, be carried out by employing the μ-synthesis approach as presented in [8].

6. CONTROLLER SYNTHESIS RESULTS

In this section, the results of the application of the fixed-structure controller synthesis methodology, presented in the previous section, to the robust chatter control problem will be presented. Delayed output feedback controllers (with $\beta = 1$ in (10)) will designed for the high-speed milling process modelled in Section 2. Firstly, a *static* delayed output feedback case will be considered in Section 6.1 for a milling process with a linear cutting model, which permits graphical illustration of the benefits of the proposed optimization-based synthesis approach because the number of controller parameters is limited in this case. Secondly, *dynamic* delayed output feedback controllers will be designed in Section 6.2 for a milling process with a nonlinear cutting model to illustrate that improved performance can be achieved by such dynamic controllers.

Here, the machine spindle-toolholder-tool dynamics, between inputs $\underline{F}_t$ and $\underline{F}_a$ and outputs $\underline{v}_t$ and $\underline{v}_a$, see Figure 3, is modelled by two decoupled subsystems (representing the dynamics in two (x, y) orthogonal directions perpendicular to the spindle axis). The dynamics in both the x-direction and y-direction are modelled as two-degree-of-freedom mass-spring-damper systems, see Figure 5, with masses $m_{i,k}$, $i \in \{a, t\}$, $k \in \{x, y\}$, with $m_{t,x}$, $m_{t,y}$ the tool mass in x-direction and y-direction, respectively, and $m_{a,x}$, $m_{a,y}$ the spindle/actuator mass in x-direction and y-direction, respectively, the eigenfrequencies $\omega_{i,k} = \sqrt{(c_{i,k}/m_{i,k})}$, $i \in \{a, t\}$, $k \in \{x, y\}$, and dimensionless damping ratios $\zeta_{i,k} = b_{i,k}/2\sqrt{(c_{i,k}m_{i,k})}$, $i \in \{a, t\}$, $k \in \{x, y\}$. This is carried out in order

DOI: 10.1002/rnc

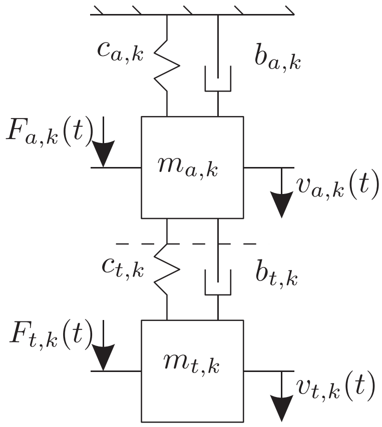

Figure 5. Spindle dynamics model, $k \in \{x, y\}$. $\underline{F}_a, \underline{v}_a$: forces, displacements at actuator. $\underline{F}_t, \underline{v}_t$: forces, displacements at tooltip.

Table I. Milling model parameters.

Parameter	Value	Parameter	Value
$m_{t,x} = m_{t,y}$	0.015 kg	K_t	462 $\left[\text{N/mm}^{(1+x_F)}\right]$
$m_{a,x} = m_{a,y}$	0.14 kg	K_r	38.6 $\left[\text{N/mm}^{(1+x_F)}\right]$
$\omega_{t,x} = \omega_{t,y}$	2350 Hz	z	4 [-]
$\omega_{a,x} = \omega_{a,y}$	1400 Hz	ϕ_s	0 [rad]
$\zeta_{t,x} = \zeta_{t,y}$	0.05 [-]	ϕ_e	π [rad]
$\zeta_{a,x} = \zeta_{a,y}$	0.12 [-]	f_z	0.2 mm/tooth

to capture the inherent dynamics between the actuator/sensor system (denoted by subscript a) and the cutting tool (denoted by subscript t). The parameters of the milling model, considered in this section, are given in Table I.

6.1. Static delayed output feedback

In this section, a static delayed output feedback controller ($n_c = 0$ and $\beta = 1$, in (10)) will be designed for the uncertain time-delay system (8). Moreover, a linear cutting model is considered (i.e., $x_F = 1$ in (3)). The structure of the controller (feedback gain) matrix is chosen such that it has a similar structure as the averaged cutting force matrix $\bar{\mathbf{H}}$, which can be written as the sum of a diagonal matrix $k\mathbf{I}$ and a skew-symmetric matrix for a linear cutting model with full immersion cutting, see [16, page 107]. Then, the controller matrix can be parametrized by only two parameters, and only two controller parameters need to be synthesized; that is, the controller matrix structure is given as

$$\mathbf{K} = \mathbf{D}_c = \begin{bmatrix} k_1 & -k_2 \\ k_2 & k_1 \end{bmatrix}, \tag{26}$$

with the unknown controller parameter vector $\underline{K}_p = \begin{bmatrix} k_1 & k_2 \end{bmatrix}^T$. This allows for a graphical representation of the results, thereby providing insight into the functioning of the optimization-based controller synthesis approach.

The static delayed output-feedback controller is designed such that it stabilizes milling operations between $n \in [36000, 38000]$ rpm, for a depth of cut, which is as large as possible given the performance requirement on the weighted control sensitivity, with a static performance weighting $W_{KS} = K_p$, where $K_p = 1 \cdot 10^{-6}$ mm/N, to limit the control action needed for stabilization. Moreover, the parameter of the penalty function is set to $\gamma = 100$, and the initial sampling radius for the gradient sampling technique is set to $\epsilon_s = 0.1$.

DOI: 10.1002/rnc

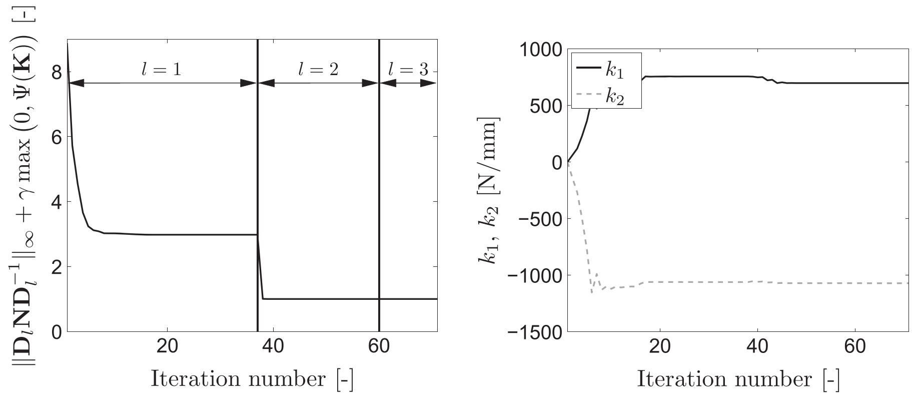

(a) Objective function.

(b) Feedback gains.

Figure 6. Objective function in K-step of algorithm (left) and feedback gains k_1 and k_2 (right) as a function of iteration number.

Starting at the initial controller parameters $k_1 = k_2 = 0$, the fixed-structure controller synthesis algorithm, as presented in Section 5, solves the constrained optimization problem (23) by iterating over $\mathbf{D}$ and $\mathbf{K}$. The algorithm converges after three D-K steps resulting in $\sup_{\omega \in \mathbb{R}} \bar{\sigma}\left(\mathbf{D}(i\omega)\mathbf{N}(i\omega)\mathbf{D}^{-1}(i\omega)\right) = 0.9992$ therewith guaranteeing robust performance for milling operations between $n \in [36000, 38000]$ rpm up to a depth of cut of $\bar{a}_p = 2.35$ mm.

In Figure 6(a), the values of the objective function during the K-step, that is, $\sup_{\omega \in \mathbb{R}} \bar{\sigma}\left(\mathbf{D}_l\mathbf{N}\mathbf{D}_l^{-1}\right) + \gamma \max(0, \Psi(\mathbf{K}))$ with $l = 1, 2, 3$ the index of the corresponding D-scale matrices $\mathbf{D}_l$, are given as function of iteration number. Moreover, the evolution of the feedback gains k_1 and k_2 during the K-steps are given in Figure 6(b). The obtained feedback gains that guarantee robust performance of the milling process for the desired uncertainties are given as

$$\begin{aligned} k_1 &= 697.1599 \,\text{N/mm}, \\ k_2 &= -1071.058 \,\text{N/mm}, \end{aligned}$$

from which it can be seen that the controller parameters are smaller than the inverse of the performance bound W_{KS}^{-1} imposed on the control sensitivity $\mathbf{KS}$. A contour plot of the objective function (24) for $\mathbf{D} = \mathbf{I}$ is given in Figure 7. Moreover, optimization history (in the first K optimization step, i.e., $l = 1$) is given in the feedback gain parameter space. It can be observed that the optimization moves toward the (local) minimum of the objective function for the given D-scaling.

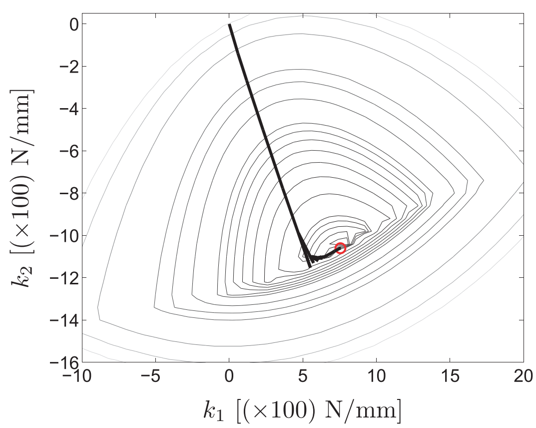

Figure 7. Contour plot of objective function (24) for fixed D-scales $\mathbf{D} = \mathbf{I}$, $\gamma = 100$ together with optimization result during the first K-step of the algorithm. The circle indicates the parameter values obtained at the end of the first K-step.

In Figure 8, a contour plot is depicted where the upper bound on $\sup_{\omega\in\mathbb{R}} \mu_{\tilde{\mathbf{\Delta}}}(\mathbf{N}(i\omega))$ is calculated for several values of k_1 and k_2. Moreover, the optimization history of the fixed-structure controller synthesis algorithm in the feedback gain parameter space is given, where the end point of each K-step in the D-K-iteration process is indicated by a circle. From the contour plot, it can be seen that during the D-K-iteration, the optimization converges to a (local) minimum thereby guaranteeing robust performance of the milling process. During the second D-K-step, the optimization moves along a non-smooth boundary of the objective function. In the same figure, the evaluation of the objective function by using the default BFGS algorithm for smooth functions (see [37, Chp. 6], invoked using `fminunc` from MATLAB) is given in grey. It can be seen that the standard BFGS algorithm gets stuck at a non-smooth boundary of the objective function (a non-smooth boundary can be distinguished from the non-smoothness of a contour).

Next, stability lobes diagrams (SLDs) are determined for the original linearized time-variant model of the milling process (Equation (8)), as outlined in Section 2.2, with and without the static delayed output-feedback controller. The SLD is given in Figure 9. It can be seen that the controller synthesis algorithm has created a peak in the SLD near the desired spindle speed range corresponding to a maximum depth of cut of $a_{p,\max} = 3.52$ in that desired spindle speed range. Note that in open loop $a_{p,\max} = 1.60$ and, thus, a 120% improvement in the chatter-free depth of cut has been achieved. Such a favorable shaping of the SLD is realized by altering the closed-loop spindle dynamics near the first resonance, see Figure 10. The fact that particularly the first resonance mode is targeted by this controller can be explained as follows. In Figure 9, it is indicated that the

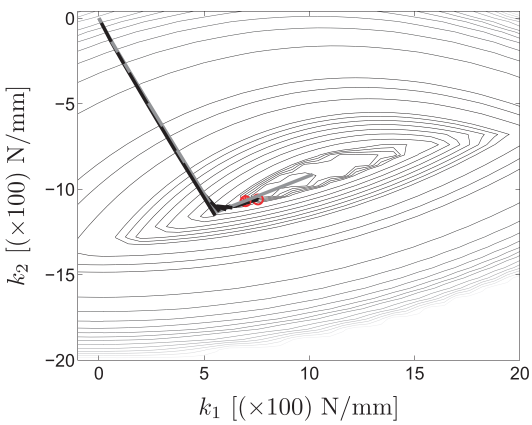

Figure 8. Contour plot of objective function $\sup_{\omega\in\mathbb{R}} \mu_{\tilde{\mathbf{\Delta}}}(\mathbf{N}(i\omega))$ together with optimization result using Algorithm 5.1 (black) and standard BFGS (grey) during three D-K-iterations of the algorithm. The circles indicate the end of each K-step.

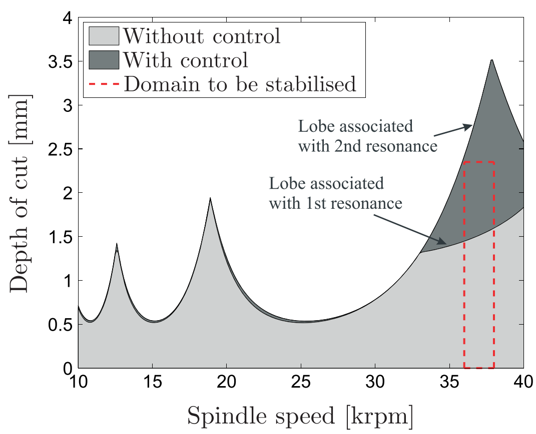

Figure 9. Stability lobes diagram with and without static output feedback controller.

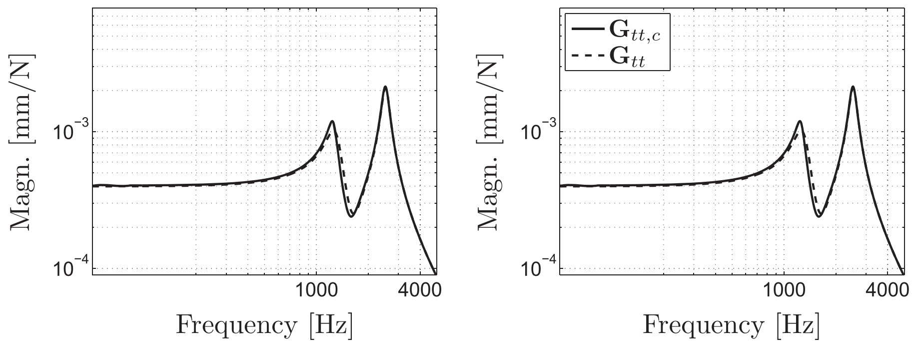

(a) Feed direction. (b) Normal direction.

Figure 10. Controlled $\mathbf{G}_{tt,c}(i\omega)$ (solid) and uncontrolled (open-loop) $\mathbf{G}_{tt}(i\omega)$ (dashed) tooltip spindle dynamics for the static-output controller designed for a range of spindle speeds, $n \in [36000, 38000]$ rpm.

SLD associated with the open-loop system is dominated, in the spindle speed range of interest, by a stability lobe corresponding to the first resonance mode of the spindle dynamics. This figure also indicates that the SLD associated with the closed-loop system is dominated, in the spindle speed range of interest, by a stability lobe corresponding to the second resonance mode of the (closed-loop) spindle dynamics. Hence, the controller ensures a shifting of the first resonance peak thereby alleviating the criticality of this resonance for the occurrence of chatter and allowing for higher chatter-free depths of cut in closed loop as evidenced in Figure 9.

Based on the discussion earlier, it can be concluded that the proposed controller synthesis strategy is able to effectively alter the SLD such that productivity is significantly increased. This is even accomplished for the least number of controller parameters. In the next section, fixed-structure controllers will be synthesized using *dynamic* delayed output-feedback controllers, thereby increasing the versatility of the controllers and the achievable performance.

6.2. Dynamic delayed output feedback

The previous section illustrated the working principle of the proposed controller design method using a static delayed output feedback controller with two controller parameters. In this section, the results will be presented by synthesizing dynamic delayed output controllers as defined by (10) (with $\beta = 1$) for $x_F = 0.744$ (i.e., for a nonlinear cutting model, see (3)). The other system parameters are taken as in Table I.

The dynamic output feedback controller will be designed such that milling operations between $n \in [34000, 36000]$ rpm are stabilized, for a depth of cut, which is as large as possible given the performance requirement on the weighted control sensitivity. Here, the performance weighting W_{KS} is chosen as

$$W_{KS}(s) = K_p \frac{\frac{1}{2\pi f_{r,l}}s + 1}{\frac{1}{2\pi f_{p,l}}s + 1} \cdot \frac{\frac{1}{2\pi f_{r,h}}s + 1}{\frac{1}{2\pi f_{p,h}}s + 1}, \tag{27}$$

with $K_p = 1 \cdot 10^{-6}$ mm/N, $f_{r,l} = 100$ Hz, $f_{r,h} = 7500$ Hz, $f_{p,l} = 1 \cdot 10^{-2}$ Hz, and $f_{p,h} = 2 \cdot 10^4$ Hz. As before, the parameter of the penalty function is set to $\gamma = 100$ and the initial sampling radius of the gradient sampling algorithm is chosen as $\epsilon_s = 0.1$.

In order to reduce the number of optimization variables (i.e., controller parameters), the initial controller, used as starting point for the optimization-based design, is transformed to the modal canonical form (herewith, the system matrix $\mathbf{A}_c$ of the reduced-order controller has the real Jordan form). After the transformation, the controller's system matrix $\mathbf{A}_c$ is a block diagonal matrix, that is, $\mathbf{A}_c = \operatorname{diag}\left(\mathbf{A}_{c,1}, \ldots, \mathbf{A}_{c,n_{\mathbb{C}}/2+n_{\mathbb{R}}}\right)$, with $n_{\mathbb{C}}$ the number of complex eigenvalues and $n_{\mathbb{R}}$ the number of real eigenvalues, and

$$\mathbf{A}_{c,l} = \lambda_l, \text{ for } \lambda_l \in \mathbb{R}, \tag{28}$$

DOI: 10.1002/rnc

and

$$\mathbf{A}_{c,l} = \begin{bmatrix} \Re(\lambda_l) & \Im(\lambda_l) \\ -\Im(\lambda_l) & \Re(\lambda_l) \end{bmatrix}, \text{ for } \lambda_l \in \mathbb{C}, \tag{29}$$

where λ_l is the solution of $\det(\lambda_l \mathbf{I} - \mathbf{A}_c) = 0$. Note that in this case, it is assumed that the eigenvalues have algebraic multiplicity one. Three fixed-structure controllers are synthesized, namely, for $n_c = 0$ (i.e., static delayed output feedback), and $n_c = 2$ and $n_c = 4$ (i.e., dynamic delayed output feedback), using the algorithm as presented in Section 5. The algorithm has to optimize 4 parameters in case of $n_c = 0$, 16 parameters in case of $n_c = 2$ and 28 parameters in case of $n_c = 4$. The results are listed in Table II. As before, SLDs are computed with the designed fixed-structure controllers and without control using the linearized time-variant model of the milling process (8), as outlined in Section 2.2. The corresponding results are given in Figure 11. For completeness, the maximal achievable depth of cut $a_{p,\max}$ from the SLD in the desired spindle speed range is listed in Table II. From the figure, it can be observed that for the case where $n_c = 0$, the fixed-structure controller indeed alters the SLD. In this case, based on the SLD, the depth of cut can be increased from $a_{p,\max} = 1.067$ mm in open loop to 1.469 mm in closed loop, which is an improvement of approximately 38%. The peak of the closed-loop stability lobe is approximately located at $n = 38700$ rpm, which is outside the domain of desired spindle speeds. Of course, if the peak of the sld could be placed inside the desired interval of spindle speeds, then a higher maximum depth of cut could be achieved. In order to shift the peak of the lobe at such a spindle speed, the controller, in this case, needs to have more complexity (freedom), which is obtained by increasing the controller order.

For the dynamic fixed-structure controllers with $n_c = 2$ and $n_c = 4$, it can be observed in Figure 11 that the SLD is altered such that a lobe is indeed created at the desired spindle speed interval. Clearly, by increasing the order of the fixed-structure controller, the area for which robust stability is guaranteed is increased. In this case, based on the SLD in Figure 11, the depth of cut can

Table II. Results from fixed-structure controller synthesis for three different controller orders; $\bar{a}_p$ denotes the maximal depth of cut for which robust performance can be guaranteed, and $a_{p,\max}$ denotes the maximal depth of cut in the SLD for the desired spindle speed interval.

n_c [-]	No. D-K-steps	$\mu_{\tilde{\mathbf{\Delta}}}$ [-]	$\bar{a}_p$ [mm]	$a_{p,\max}$
0	7	0.9983	1.1250	1.4690
2	10	0.9918	1.8250	2.1456
4	9	0.9810	2.0000	2.3992

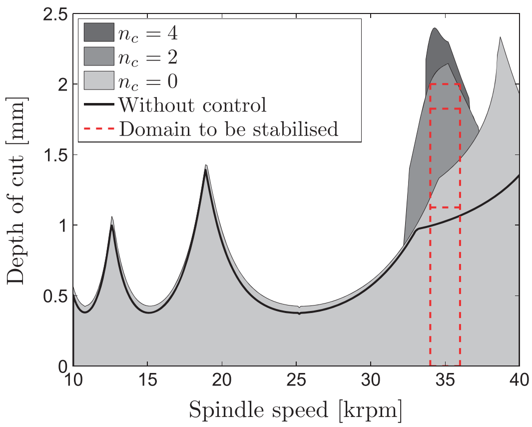

Figure 11. Stability lobes diagram for the structured delayed dynamic output feedback controllers for 0, 2, and 4 controller states, respectively, and without control. The area for which robust stability is guaranteed is indicated by the dashed boxes, see also Table II.

DOI: 10.1002/rnc

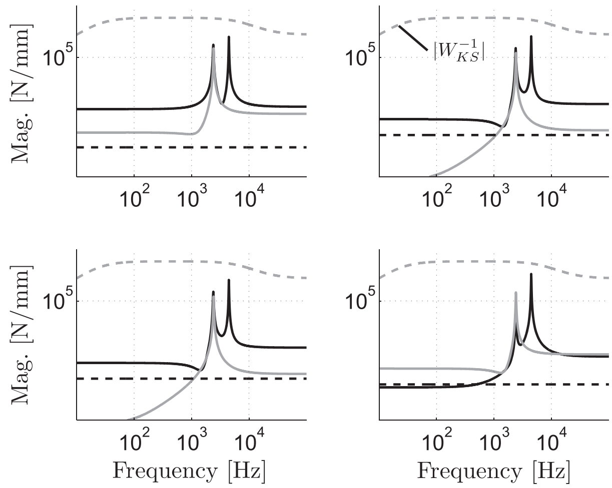

Figure 12. Magnitude of the fixed-structure controller for $n_c = 0$ (black dashed), $n_c = 2$ (grey solid), and $n_c = 4$ (black solid) controller states, which stabilizes the milling process for $n \in [34000, 36000]$ rpm. Also, the magnitude of the inverse of the performance weighting function W_{KS} is given.

be increased from $a_{p,\max} = 1.067$ mm to $a_{p,\max} = 2.146$ for $n_c = 2$ and to $a_{p,\max} = 2.399$ for $n_c = 4$, which leads to a productivity increase of approximately 101% and 125%, respectively.

The resulting fixed-structure controllers are given in Figure 12. From the figure, it can be seen that the controllers designed for $n_c = 2$ and $n_c = 4$ are dynamic MIMO controllers with notch characteristics. The closed-loop tooltip dynamics in both x-direction and y-direction are given in Figure 13. In the same figure, the interval of tooth passing excitation frequencies f_{tpe} associated with the spindle speed interval $n \in [34000, 36000]$ rpm is indicated. It can be seen that the static controller, that is, $n_c = 0$, mainly changes the dynamics around the first resonance peak (at around 1300 Hz), see related discussion in Section 6.1. For the dynamic fixed-structure controllers with $n_c = 2$ and $n_c = 4$, it can be observed that the controllers also alter the closed-loop tooltip spindle dynamics such that the second resonance (at around 2500 Hz) is shifted to a lower frequency range. This second resonance is altered such that it lies inside the area of desired tooth passing excitation frequencies, which is beneficial for stability. The fact that a closed-loop spindle resonance situated at a tooth-passing excitation frequency is beneficial for avoiding chatter can be explained as follows. In the milling process, the highest depth of cut can be obtained (corresponding to a peak in the SLD) when the dynamic chip thickness $h_{j,\text{dyn}}(t) = \underline{v}_t(t) - \underline{v}_t(t-\tau)$ is equal to zero. This relation can be transformed to the frequency domain as follows:

$$\underline{H}_{j,\text{dyn}}(\mathrm{i}\omega) = (1 - e^{-\mathrm{i}\omega\tau})\underline{V}_t(\mathrm{i}\omega) =: Q(\mathrm{i}\omega)\underline{V}_t(\mathrm{i}\omega), \tag{30}$$

where $\underline{H}_{j,\text{dyn}}(\mathrm{i}\omega)$ and $\underline{V}_t(\mathrm{i}\omega)$ are the Fourier transforms of $h_{j,\text{dyn}}(t)$ and $\underline{v}_t(t)$, respectively. Hence, the difference between the tooltip displacements of the present and previous cut is actually characterized by a filter, denoted by $Q(\mathrm{i}\omega)$, with zeros at $\omega = l\frac{2\pi}{\tau} = l2\pi f_{tpe}, l = 0, 1, 2, \ldots$ (and f_{tpe} the tooth-passing frequency). Moreover, for the milling process, the dominant (chatter) frequency of the perturbation vibrations lies in general close to a resonance frequency of the spindle dynamics. Then, by designing the controller such that the dominant closed-loop resonance frequency is close to a tooth-passing frequency and due to the filter properties of the $Q(\mathrm{i}\omega)$ (in particular the location of the zeros of $Q(\mathrm{i}\omega)$ at f_{tpe}-related frequencies), the dynamic chip thickness is enforced to be zero at the desired spindle speed. This, in turn, results in a large depth of cut within the desired spindle speed range and a peak in the SLD at that spindle speed (see Figure 11 for $n_c = 2$ and $n_c = 4$). So, by applying robust control design techniques, a controller is designed, which tailors the tooltip spindle dynamics, such that a resonance is created near a tooth passing harmonic, which in turn results in a peak in the SLD and a high increase in productivity.

Remark. We care to stress that the fact that a closed-loop resonance is close to a tooth-passing frequency only applies to the closed-loop dynamics (8), (9), (10) in perturbation coordinates and not

DOI: 10.1002/rnc

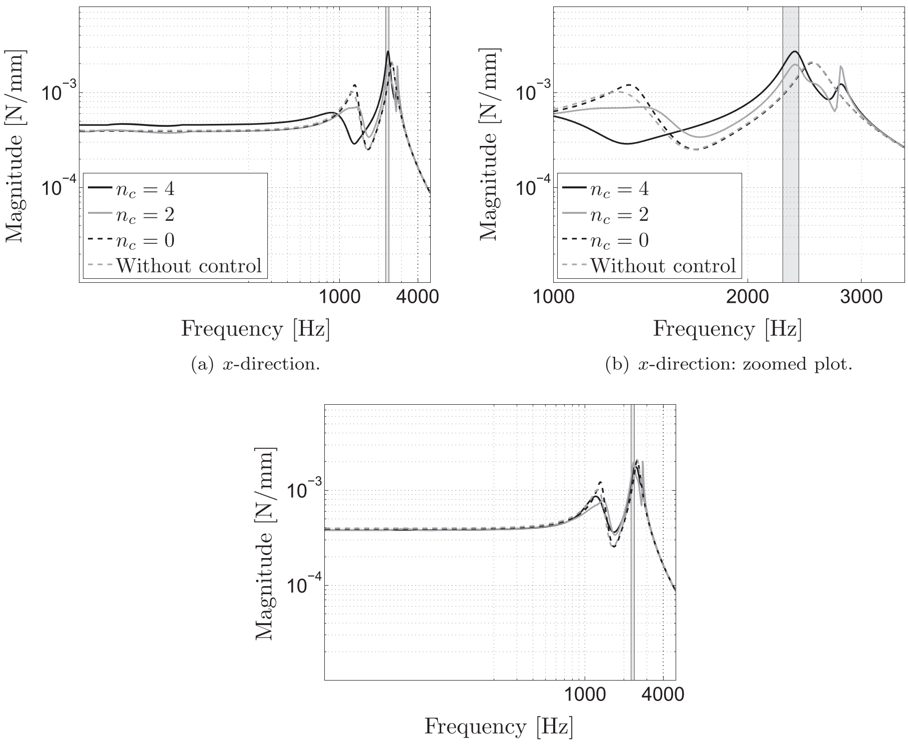

(a) x-direction.

(b) x-direction: zoomed plot.

(c) y-direction.

Figure 13. Controlled $\mathbf{G}_{tt,c}(i\omega)$ and uncontrolled $\mathbf{G}_{tt}(i\omega)$ tooltip spindle dynamics in x-direction and y-direction for fixed-structure controller for $n_c = 0, n_c = 2$ and $n_c = 4$ states designed for a spindle speed interval $n \in [34000, 36000]$ rpm. The interval of tooth passing excitation frequencies corresponding to the spindle speed range is indicated by the grey area.

to the dynamics (7) governing the underlying periodic solution $x^*(t)$ associated with the 'no-chatter' milling response. The latter statement is valid by the grace of the fact that the proposed controller only employs feedback of the perturbation variables, see (10), and hence the control action vanishes on the nominal periodic (no-chatter) solution $x^*(t)$. As a consequence, this nominal solution is not changed by the controller and the fact that a closed-loop resonance of the *perturbation* dynamics is close to a tooth-passing frequency does not imply that the *nominal* solution is subject to (undesired) resonance phenomena.

Related to this, we remark that if the controller would not be based on perturbation feedback, the controller may affect the nominal solution, which, in turn, may become associated with resonance-induced high-amplitude vibrations. Clearly, the latter scenario is generally undesired, and this further motivates the usage of perturbation feedback and its implementation through Pyragas-type delayed feedback. Finally, we note that if high-amplitude nominal vibrations would be induced, other models for the chip thickness than that employed in this paper may be needed, as indicated in [43].

7. CONCLUSIONS

This paper proposes a methodology to synthesize fixed-structure controllers guaranteeing robust stability and performance of the high-speed milling process, in particular, the avoidance of chatter in a predefined area of depth-of-cut and spindle speed while respecting limitations regarding the required actuator forces. The resulting controllers are of low complexity (order) and facilitate a significant increase in the feasible material removal rate.

The controller synthesis problem has been cast into a non-smooth constrained optimization problem, which can be transformed to an unconstrained non-smooth optimization problem using a

DOI: 10.1002/rnc

penalty function. The unconstrained optimization problem is solved using D-K-iteration. The K-step is solved by utilizing a dedicated non-smooth optimization algorithm based on bundle methods.

An important aspect of the proposed controller structure is the choice of the measurement variable used for feedback. Here, we have proposed delayed dynamic output-feedback controllers for chatter mitigation in high-speed milling. The employment of delayed output feedback simplifies the implementation of the active chatter control procedure in practice as no additional estimators for chatter-related vibrations are needed. Moreover, the approach enables the design of relatively low-order controllers, which is desirable from a real-time implementation perspective especially given the high-frequency characteristics of the milling dynamics. The presented examples illustrate the power of the proposed controller synthesis methodology in terms of ensuring a significantly higher material removal rate in closed loop while avoiding chatter.

The real-life implementation of the control strategy proposed here gives rise to mechatronic design challenges related to specifications on sensors, actuators, and computational platforms, and further research is needed to experimentally validate the proposed control strategy in practice. For industrial implementation of the proposed control strategy, an adapted machine tool design should be pursued including integrated actuators and sensors. The design of such spindles is a challenging topic for future work. Nevertheless, prototype spindles have been developed already (see, e.g., [3, 4, 7, 44]) for such purpose. The latter fact illustrates the feasibility of applying advanced chatter control strategies, such as that developed in this paper, in practice.

ACKNOWLEDGEMENTS

This work is supported by the Dutch Ministry of Economic Affairs, Agriculture and Innovation within the framework of Innovation Oriented Research Programmes (IOP) Precision Technology.

REFERENCES

1. Liu KJ, Rouch KE. Optimal passive vibration control of cutting process stability in milling. *Journal of Materials Processing Technology* 1991; **28**(1-2):285–294.
2. Tarng YS, Kao JY, Lee EC. Chatter suppression in turning operations with a tuned vibration absorber. *Journal of Materials Processing Technology* 2000; **105**(1):55–60.
3. Dohner JL, Lauffer JP, Hinnerichs TD, Shankar N, Regelbrugge ME, Kwan CM, Xu R, Winterbauer B, Bridger K. Mitigation of chatter instabilities in milling by active structural control. *Journal of Sound and Vibration* 2004; **269**(1-2):197–211.
4. Kern S, Ehmann C, Nordmann R, Roth M, Schiffler A, Abele E. Active damping of chatter vibrations with an active magnetic bearing in a motor spindle using μ-synthesis and an adaptive filter. *The 8th International Conference on Motion and Vibration Control*, Daejeaon, Korea, 2006.
5. Zhang Y, Sims ND. Milling workpiece chatter avoidance using piezoelectric active damping: a feasibility study. *Smart Materials and Structures* 2005; **14**(6):N65–N70.
6. Shiraishi M, Yamanaka K, Fujita H. Optimal control of chatter in turning. *International Journal of Machine Tools and Manufacture* 1991; **31**(1):31–43.
7. Chen M, Knospe CR. Control approaches to the suppression of machining chatter using active magnetic bearings. *IEEE Transactions on Control Systems Technology* 2007; **15**(2):220–232.
8. van Dijk NJM, van de Wouw N, Doppenberg EJJ, Oosterling JAJ, Nijmeijer H. Robust active chatter control in the high-speed milling process. *IEEE Transactions on Control Systems Technology* 2011; **20**(4):901–917.
9. van Dijk NJM. Active chatter control in high-speed milling processes. *Ph.D. Thesis*, Eindhoven University of Technology, 2011. (Available from: http://www.dct.tue.nl/New/Wouw/phdthesisvandijk2011.pdf) [Accessed on 23 November 2014].
10. van Dijk NJM, Doppenberg EJJ, Faassen RPH, van de Wouw N, Oosterling JAJ, Nijmeijer H. Automatic in-process chatter avoidance in the high-speed milling process. *Journal of Dynamic systems, Measurement and Control* 2010; **132**(3):031006 (14 pages).
11. Pyragas K. Continuous control of chaos by self-controlling feedback. *Physics Letters A* 1992; **170**(6):421–428.
12. Fridman E, Shaked U. Delay-dependent stability and H_∞ control: constant and time-varying delays. *International Journal of Control* 2003; **76**(1):48–60.
13. Apkarian P, Noll D. Nonsmooth H_∞ synthesis. *IEEE Transactions on Automatic Control* 2006; **51**(1):71–86.
14. Michiels W, Niculescu SI. *Stability and Stabilization of Time-Delay Systems: An Eigenvalue-Based Approach*. SIAM: Philadelphia, USA, 2007.
15. van Dijk NJM, van de Wouw N, Nijmeijer H. Low-order control design for chatter suppression in high-speed milling. *Proceedings of the Conference on Decision and Control*, Orlando, FL, USA, 2011; 663–668.
16. Altintas Y. *Manufacturing Automation*. Cambridge University Press: Cambridge, UK, 2000.

DOI: 10.1002/rnc

17. Faassen RPH, van de Wouw N, Oosterling JAJ, Nijmeijer H. Prediction of regenerative chatter by modelling and analysis of high-speed milling. *International Journal of Machine Tools and Manufacture* 2003; **43**(14):1437–1446.
18. Stépán G. Modelling nonlinear regenerative effects in metal cutting. *Philosophical Transactions of the Royal Society A: Mathematical, Physical and Engineering Sciences* 2001; **359**(1781):739–757.
19. Insperger T, Stépán G, Bayly PV, Mann BP. Multiple chatter frequencies in milling processes. *Journal of Sound and Vibration* 2003; **262**(2):333–345.
20. Olgac N, Sipahi R. Dynamics and stability of variable-pitch milling. *Journal of Vibration and Control* 2007; **13**(7):1031–1043.
21. Merritt HE. Theory of self-excited machine-tool chatter. *Journal of Engineering for Industry* 1965; **87**(4):447–454.
22. Knospe C. Active magnetic bearings for machining applications. *Control Engineering Practice* 2007; **15**(3):307–313.
23. Faassen RPH, van de Wouw N, Nijmeijer H, Oosterling JAJ. An improved tool path model including periodic delay for chatter prediction in milling. *Journal of Computational and Nonlinear Dynamics* 2007; **2**(2):167–179.
24. Farkas M. *Periodic Motions*. Springer-Verlag: Berlin, 1994.
25. Insperger T, Stépán G. Updated semi-discretization method for periodic delay-differential equations with discrete delay. *International Journal for Numerical Methods in Engineering* 2004; **61**(1):117–141.
26. Michiels W, Fridman E, Niculescu SI. Robustness assessment via stability radii in delay parameters. *International Journal of Robust and Nonlinear Control* 2009; **19**:1405–1426.
27. Huang YP, Zhou K. Robust stability of uncertain time-delay systems. *IEEE Transactions on Automatic Control* 2000; **45**(11):2169–2173.
28. Zhou K, Doyle JC, Glover K. *Robust and Optimal Control*. Prentice Hall: Upper Saddle River, USA, 1996.
29. Packard A, Doyle J. The complex structured singular value. *Automatica* 1993; **29**(1):71–109.
30. The MathWorks, Inc. http://www.mathworks.com [Accessed on 23 November 2014].
31. Young P, Newlin M, Doyle J. Practical computation of the mixed μ problem. *Proceedings of the American Control Conference*, Vol. 3, Chicago, IL, USA, 1992; 2190–2194.
32. Wolfe P. A method of conjugate subgradients for minimizing nondifferentiable functions. In *Nondifferentiable Optimization*, vol. 3, Balinski ML, Wolfe P (eds)., Mathematical Programming Study. Elsevier: Amsterdam, the Netherlands, 1975; 145–173.
33. Hiriart-Urruty JB, Lemaréchal C. *Convex Analysis and Minimization Algorithms II: Advanced Theory and Bundle Methods*. Springer-Verlag: Berlin, 1993.
34. Burke J, Lewis A, Overton M. A robust gradient sampling algorithm for nonsmooth, nonconvex optimization. *SIAM Journal on Optimization* 2005; **15**(3):751–779.
35. Burke J, Lewis A, Overton M. Two numerical methods for optimizing matrix stability. *Linear Algebra and its Applications* 2002; **351-352**:117–145.
36. Lewis A, Overton M. Hybrid algorithm for nonsmooth optimization HANSO, 2010. (Available from: http://www.cs.nyu.edu/faculty/overton/software/hanso/index.html) [Accessed on 23 November 2014].
37. Nocedal J, Wright S. *Numerical Optimization* (Second). Springer: New York, USA, 2006.
38. Luenberger D. *Linear and Nonlinear Programming* (Third), Vol. 116. Springer: New York, USA, 2008.
39. Bruinsma N, Steinbuch M. A fast algorithm to compute the H_∞-norm of a transfer function matrix. *Systems & Control Letters* 1990; **14**(4):287–293.
40. Gumussoy S, Michiels W. Computing $\mathcal{H}_\infty$ norms of time-delay systems. *Joint 48th IEEE Conference on Decision and Control and 28Th Chinese Control Conference*, Shanghai, China, 2009; 263–268.
41. Engelborghs K, Luzyanina T, Samaey G. Dde-biftool v. 2.00: a matlab package for bifurcation analysis of delay differential equations: TW Report 330, Department of Computer Science, Katholieke Universiteit Leuven: Belgium, 2001.
42. Altintas Y, Weck M. Chatter stability of metal cutting and grinding. *CIRP Annals - Manufacturing Technology* 2004; **53**(2):619–642.
43. Bachrathy D, Stépán, Turi J. State dependent regenerative effect in milling processes. *Journal of Computational and Nonlinear Dynamics* 2011; **6**:041002–1/041002–9.
44. Ries M, Pankoke S, Gebert K. Increase of material removal rate with an active hsc milling spindle. *In Proceedings of the Adaptronic Congress*, Göttingen, Germany, 2006.